A Quantitative Comparison of Simultaneous BOLD fMRI and NIRS Recordings during Functional Brain Activation

Gary Strangman,*,†,‡ Joseph P. Culver,† John H. Thompson,† and David A. Boas†

*Neural Systems Group and †NMR Center, Massachusetts General Hospital–Harvard Medical School, and
‡Harvard–MIT Division of Health Sciences and Technology, Charlestown, Massachusetts 02129

Near-infrared spectroscopy (NIRS) has been used to noninvasively monitor adult human brain function in a wide variety of tasks. While rough spatial correspondences with maps generated from functional magnetic resonance imaging (fMRI) have been found in such experiments, the amplitude correspondences between the two recording modalities have not been fully characterized. To do so, we simultaneously acquired NIRS and blood-oxygenation level-dependent (BOLD) fMRI data and compared $\Delta(1/\text{BOLD})$ ($\approx R_2^*$) to changes in oxyhemoglobin, deoxyhemoglobin, and total hemoglobin concentrations derived from the NIRS data from subjects performing a simple motor task. We expected the correlation with deoxyhemoglobin to be strongest, due to the causal relation between changes in deoxyhemoglobin concentrations and BOLD signal. Instead we found highly variable correlations, suggesting the need to account for individual subject differences in our NIRS calculations. We argue that the variability resulted from systematic errors associated with each of the signals, including: (1) partial volume errors due to focal concentration changes, (2) wavelength dependence of this partial volume effect, (3) tissue model errors, and (4) possible spatial incongruence between oxy- and deoxyhemoglobin concentration changes. After such effects were accounted for, strong correlations were found between fMRI changes and all optical measures, with oxyhemoglobin providing the strongest correlation. Importantly, this finding held even when including scalp, skull, and inactive brain tissue in the average BOLD signal. This may reflect, at least in part, the superior contrast-to-noise ratio for oxyhemoglobin relative to deoxyhemoglobin (from optical measurements), rather than physiology related to BOLD signal interpretation. © 2002 Elsevier Science (USA)

Key Words: near-infrared spectroscopy; functional magnetic resonance imaging; oxyhemoglobin; deoxyhemoglobin; T_2^*.

INTRODUCTION

Diffuse optical methods for noninvasive brain monitoring have been in use for nearly 25 years (Jobsis, 1977) and are made possible by the fact that both oxyhemoglobin (HbO₂) and deoxyhemoglobin (HbR) are chromophores with useful optical properties. Specifically, near-infrared light between 650 and 950 nm is remarkably weakly absorbed by biological tissue, and the absorption spectra of HbR and HbO₂ differ substantially in this range (cf. Sfareni *et al.,* 1997; Wray *et al.,* 1988). Together these properties make possible the noninvasive spectroscopic determination of HbR and HbO₂ concentrations *in vivo* from diffusely scattered light. Such measurements can be made on a variety of tissues, including on the head during functional brain activation (e.g., Adelson *et al.,* 1998; Fantini *et al.,* 1994; Gratton *et al.,* 1995; Hock *et al.,* 1995; Obrig *et al.,* 1996; Wolf *et al.,* 1997). While diffuse optical measurements are poorer in spatial resolution and depth penetration than functional magnetic resonance imaging (MRI), they have the advantage of providing information about HbR, HbO₂, and total hemoglobin (HbT), as well as a high temporal resolution for detailed investigation of physiological rhythms. These advantages can be used to better understand the nature of the baseline physiology, the hemodynamic response to neuronal activation, and the origin of the blood-oxygenation level-dependent (BOLD) signal.

At present, there are two main limitations of optical techniques. First, as with several other noninvasive brain imaging methods (e.g., EEG, MEG, PET), anatomical information is not directly obtained, making difficult the localization of externally recorded signals with respect to the underlying brain. External landmarks can be used for probe localization (Homan *et al.,* 1987; Steinmetz *et al.,* 1989), but these landmarks offer only probabilistic guidelines for inferences about location. The second limitation, which is more problematic, arises from errors in the photon diffusion model required for calculating hemoglobin species concentrations. The sensitivity of a given optical measurement to

the tissue layers beneath an optical probe, including sensitivity to brain tissue, is still poorly understood. Moreover, it remains unclear just how susceptible the calculations of HbR and HbO_2 are to model errors arising from the simplified tissue geometries that are typically assumed. As a consequence, the reliable quantification of absolute HbR and HbO_2 concentrations is still lacking.

Simultaneously acquired optical and MRI data have the potential to overcome both limitations. First, simultaneous recordings address the localization limitation by providing information about where the optical probes lay with respect to the underlying brain, thereby allowing investigation of spatial correspondences between recording modalities. This was initially demonstrated by Kleinschmidt et al. (1996), who showed qualitative spatial specificity of near-infrared spectroscopy (NIRS) using a single source–detector pair for the optical measurements. Similar qualitative spatial specificities have also been obtained by Benaron et al. (2000) and Cannestra et al. (2001). Toronov and collaborators also showed qualitative spatial correspondences between BOLD functional (f) MRI measures and optically derived signals, as well as qualitative temporal correspondences between the two signals using both amplitude measures (Toronov et al., 2001a) and phase measures (Toronov et al., 2001b). Detailed amplitude correspondence measures have not yet been reported.

Simultaneous MR–optical recordings address the second limitation by providing anatomical information necessary to improve optical models. Given appropriate computational tools and MR images, the anatomical MR data can be segmented into tissue types and, following coregistration of the optical probe with the anatomical MR scan, theoretical Monte Carlo simulations can be performed to determine the sensitivity of particular source–detector pairs to regions of that subject's brain. Recently, such Monte Carlo approaches have been undertaken to describe theoretical sensitivity profiles to underlying visual cortex, suggesting that brain motion and/or pial vessels might account for some of the optical sensitivity (Firbank et al., 1998). Sensitivity profiles could also be used as an anatomical prior for reconstructing optical images of brain activity at better spatial resolution.

Overcoming the current limitations of optical techniques will allow one to more carefully address the issue of quantifying hemoglobin species concentrations. Thus far, the closest approach to quantitation has been achieved only in animal models. For example, in an invasive (scalp-removed) piglet preparation, Punwani et al. (1997, 1998) simultaneously acquired MRI and NIRS data and demonstrated a strong positive linear relationship between $R_2^* = 1/T_2^*$ and [HbR] during carbon dioxide challenge. The invasive preparation reduces the known difficulties with quantitation given

focal activations (Boas et al., 2001). However, it impinges on an incompletely understood, interim scattering regime in which the detected light is neither singly scattered nor fully diffuse (Nolte et al., 1998; Simpson et al., 1998)—leaving partially open the question of how accurate the [HbR] values are. Importantly, neither HbO_2 nor HbT was considered in those studies.

To begin to fill in the gaps between the human and the animal work, we compared and quantified the relationships between BOLD fMRI signal change and the changes in all three hemoglobin species—HbR, HbO_2, and HbT—as they evolve over time during noninvasive, adult human brain recording. To do this required a simultaneous-recording paradigm and an examination of the assumptions of existing models on the quantification of [HbR] and [HbO_2] via NIRS. After accounting for individual differences, we found strong correlations between $\Delta(1/BOLD)$ ($\approx R_2^*$) and all hemoglobin parameters. We discuss the reasons for differences across hemoglobin species, as well as the possibilities for the development of MR–optical synergies, including the benefits gained by MR from simultaneous MR–optical recordings.

METHODS

Subjects

Three subjects underwent simultaneous functional MR scanning and diffuse optical recording. All were strongly right handed, as determined by the Oldfield Handedness Inventory (Oldfield, 1971). The study was approved by the institutional review board at the Massachusetts General Hospital, where the experiments were performed, and all subjects gave their written informed consent.

Diffuse Optical

Diffuse optical recordings were performed using a custom-built instrument with 16 detector and 9 source locations. Two colors were emitted at each source location, and the associated 18 lasers were frequency encoded (4–7 kHz) to enable simultaneous operation. Source fibers were bifurcated glass fiber bundles, with 2.7-mm core diameter and 10 m in length (Fiberoptics Technology, prototype), coupled to laser diodes emitting at 786 (Sanyo, DL7140-201) and 830 nm (Hitachi, HL8325G). Detectors consisted of avalanche photodiode modules (Hamamatsu C5460-01), also coupled to glass fiber bundles (2.7-mm core diameter). The bandwidth for each source–detector pair was 3 Hz and was digitized at 30 Hz. The flexible fiber-holder probe was positioned roughly centered over the C3 location in the international 10–20 system (Homan et al., 1987).

Magnetic Resonance

After being fitted with the optical apparatus, subjects were positioned for MR scanning. All MR imaging was performed on a Siemens Sonata 1.5-T scanner (Siemens Corp.). Three anatomical sequences were run, including a 3D-SPGR sequence (TR = 7.25 ms, TE = 3.2 ms, $\theta = 7°$, $1 \times 1 \times 1.33$-mm resolution), a T_2-weighted fast spin-echo sequence (TR = 10 s, TE = 48 ms, $\theta = 120°$, 27 slices, 5 mm thick, 0.75-mm skip, 0.9375×0.9375-mm in-plane resolution), and a whole-brain T_1-weighted echo-planar sequence (TR = 8 s, TE = 39 ms, $\theta = 90°$, 27 slices, 5 mm thick, 0.75-mm skip, 3.125×3.125-mm in-plane resolution). Functional imaging was performed with gradient-echo BOLD–EPI sequences, collected in the same planes as the T_1 images (TR = 2.5 s, TE = 40 ms, $\theta = 90°$, 27 slices, 5 mm thick, 0.75-mm skip, 3.125×3.125-mm in-plane resolution). One such BOLD scan was run per motor rate investigated.

Behavioral Protocol

After anatomical scanning, each subject was asked to perform a four-finger flexion/extension task. The task alternated resting periods with flexion/extension of the four fingers of a designated hand at a rate paced by a blinking asterisk. Three runs were performed per subject, one each at an asterisk blink rate of 1, 2, and 3 Hz. The 15-s periods of activation were alternated with 15-s periods of rest, and signals were recorded continuously for a run of 255 s (eight active periods, nine resting periods).

Data Analysis

Functional MR scans were first motion-corrected (AFNI, Robert Cox, NIH) and then coregistered with each anatomical scan. Analyses were within subject, and hence no spatial normalization or coordinate transformation procedures were applied. Functional maps were generated by simple Student t tests comparing active versus rest periods, time shifted by 2 TRs (5 s) to compensate for the delayed rise time of the hemodynamic response. A simple P-value threshold at $P < 0.05$ (Bonferroni corrected) was used to determine regions of activation.

For coregistration of optical and MR data, fiducial markers on each detector fiber were identified in the MR coordinate space, along with the corresponding slight field-plus-surface inhomogeneity generated by the optical fiber tip. For comparative analysis of MR and optical time series, the fMRI-defined region of activation closest to the scalp was identified, and all side-connected voxels within that region were selected as the region of interest. These "shallowest" activated voxels were assumed to be those to which the optical measurement would be most sensitive. The source–

detector pair closest to the region of interest (i.e., the one that was *a priori* presumed to have the highest sensitivity to that region of cortex) was chosen as the appropriate source for comparison with optical signals for each subject.

Optical data from individual source–detector pairs were analyzed using the modified Beer–Lambert law (MBLL), which is an empirical description of optical attenuation in a highly scattering medium (Cope *et al.,* 1987). A change in chromophore concentration causes the detected light intensity to change and, according to the MBLL, this change can be represented as

$$\Delta\text{OD} = -\ln\frac{I_{\text{Final}}}{I_{\text{Initial}}} = \varepsilon B L \Delta C, \tag{1}$$

where $\Delta\text{OD} = \text{OD}_{\text{Final}} - \text{OD}_{\text{Initial}}$ is the change in optical density (the logarithm is base e), I_{Final} and I_{Initial} are the measured intensities before and after the concentration change, and ΔC is the change in concentration. L is specified by the probe geometry (equaling the source–detector separation), ε is the extinction coefficient, and B is the differential pathlength factor (DPF; Kohl *et al.,* 1998). B can be determined from independent measurements with a time-domain system and has been tabulated for various tissues (Delpy and Delpy, 1988; Essenpreis *et al.,* 1993; Duncan *et al.,* 1995, 1996). To determine the contribution of multiple chromophores, we must take measurements at one or more wavelengths per chromophore to be resolved. We can then rewrite Eq. (1) as

$$\Delta\text{OD}(\lambda) = (\varepsilon_{\text{HbO}_2}(\lambda)\Delta[\text{HbO}_2] \\ + \varepsilon_{\text{HbR}}(\lambda)\Delta[\text{HbR}])B(\lambda)L, \tag{2}$$

where λ indicates a particular wavelength. Equation (2) explicitly accounts for independent concentration changes in oxyhemoglobin ($\Delta[\text{HbO}_2]$) and deoxyhemoglobin ($\Delta[\text{HbR}]$). By measuring ΔOD at two wavelengths (λ_1 and λ_2) and using the known extinction coefficients of oxyhemoglobin ($\varepsilon_{\text{HbO}_2}$) and deoxyhemoglobin ($\varepsilon_{\text{HbR}}$) at those wavelengths, we can then separately determine the concentration changes of oxyhemoglobin and deoxyhemoglobin (the generalization of this formula for more than two wavelengths can be found in Cope *et al.,* 1991).

Applications of the MBLL approximation typically assume that any hemodynamic change in tissue is *global* within the sampled region (Cope and Delpy, 1988; Cope *et al.,* 1991)—an assumption that is seriously violated in noninvasive brain imaging applications. In particular, functional activation in the brain is expected to occur largely (if not exclusively) in brain gray matter. This tissue layer both is thin (a few millimeters) and resides 1–2 cm below the surface of the
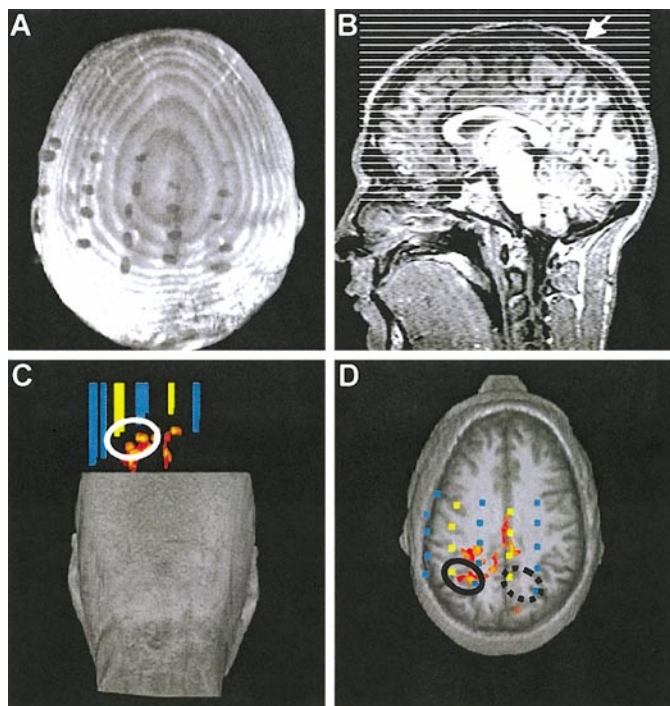
FIG. 1. Coregistration of MR and optical datasets for subject 1. (A) Fiducial markers rendered with respect to the subject's head. (B) Location of the axial fMRI slices, and an example of the irregularities caused by optical fiber tips (arrow). (C and D) Functional activation and optical fiber locations rendered in 3D, with an anatomical cutaway. Source fibers appear in yellow, detector fibers in blue. Solid circles represent the chosen activated region for this subject (source 5, detector 6); dotted circle corresponds to the adjacent inactive region investigated.

irregularity (arrow) induced by the fiber tips. Functional renderings (Figs. 1C and 1D, two views of the same data) plus coregistration provided the information necessary to select the most superficial activated brain region in each subject and the corresponding optical source–detector pair. The identified regions of MR activation that were closest to the scalp were in the superior parietal lobule (BA 7), primary motor cortex (BA 4), and premotor cortex (BA 6) for subjects 1, 2, and 3, respectively. All voxels in these three regions were strongly activated ($P < 10^{-6}$, uncorrected).

Figure 2 shows one example of the raw time series, recorded from subject 1 at the 3-Hz motor rate. Optical data at 786 and 830 nm for the pair consisting of source 5/detector 6 (Fig. 1, solid circle) is displayed in optical density change units (ΔOD) units (natural log), with

scalp, depending on the person and location on the head. By itself, this focal effect would simply result in an underestimation of species concentration changes. However, since different colors of light penetrate to different depths, each color will typically also have different mean pathlengths through an activated region of gray matter. If appropriately corrected B values are not used, the consequence is cross talk between hemoglobin species—changes in HbO_2 interpreted as changes in HbR and vice versa (Boas *et al.,* 2001). In this paper, we simply applied the MBLL using three different pairs of pathlength correction factors to examine the sensitivity of our findings to the unknown pathlength parameters. A more rigorous approach is considered in the Discussion.

RESULTS

Figure 1 illustrates the fiducial markers (Fig. 1A), the locations of MR imaging slices (Fig. 1B), and the coregistration of optodes and fMRI maps (Figs. 1C and 1D), all overlaid on renderings from the 3D-SPGR MR images. Each fiber position and orientation could be determined from the fiducial marker plus the scalp
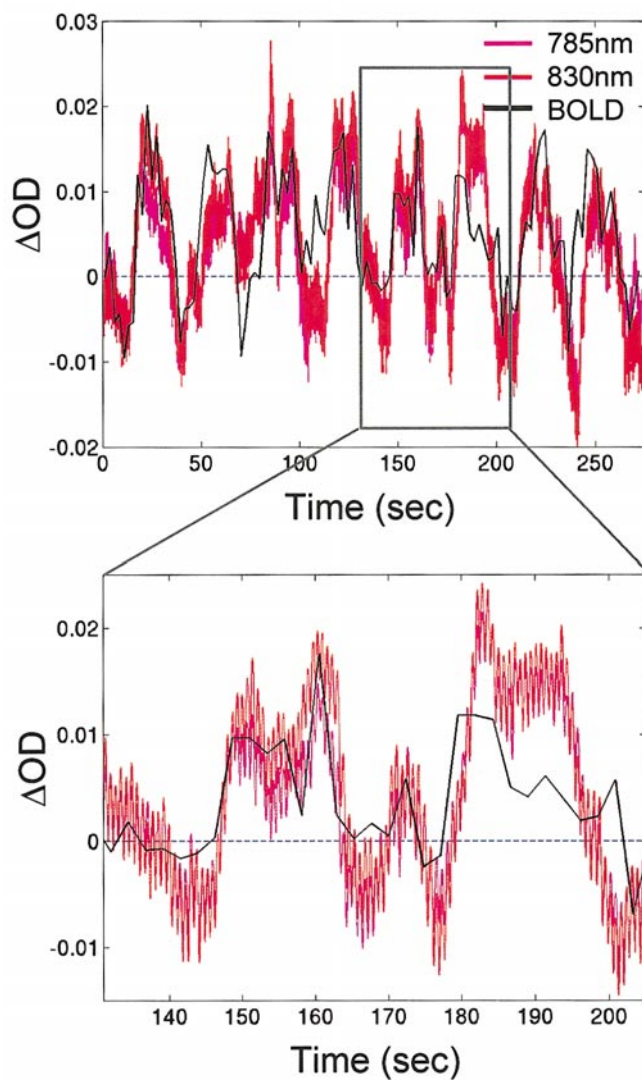

FIG. 2. Top: Raw optical and MR time series for an entire 275-s experimental run (3 Hz, subject 1) for the source–detector pair over a region of activation. Bottom: An expanded time base for 75 s of the run showing the temporal details of the optical signal.
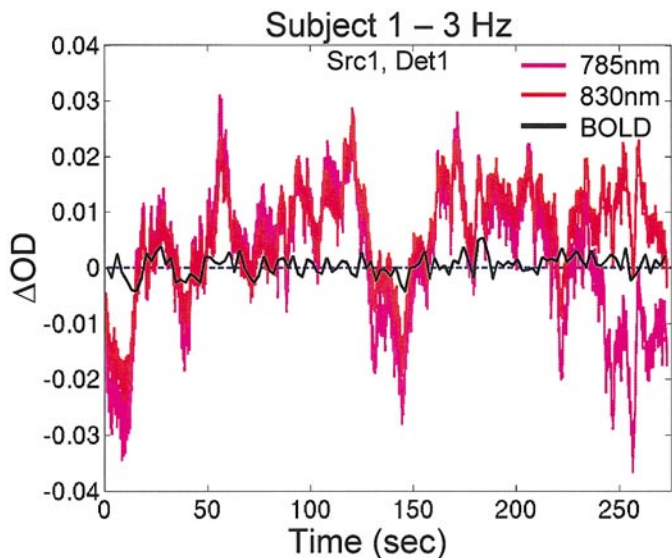
FIG. 3. Raw time series for the same run as in Fig. 2, showing data from the source–detector pair over the inactive region (see Fig. 1) and the corresponding average MR response over four brain voxels below and between this pair.

increases thereby indicating an increase in absorption. The MR time series—an average over four voxels localized to the superior parietal lobule—is plotted in percentage change units, scaled to match the amplitude of the optical data. (Actual peak percentage change in BOLD signal was 5%). The two signals are clearly related despite the potential for optical sensitivity to global changes in overlying tissues described by Firbank *et al.* (1998).

The lower portion of Fig. 2 provides additional temporal detail for the optical signal and highlights the fact that the apparent noise in the longer optical time series is actually heart-rate oscillation (frequency ~1.1 Hz) and hence physiological variation, not optical measurement noise. The oscillations with a period of approximately 10 s may reflect Mayer waves (Mayhew *et al.,* 1996; Taylor *et al.,* 1998), although such low-frequency phenomena in humans have only recently been described in detail (Obrig *et al.,* 2000) and therefore the sources of these signals are still under investigation. Figure 3 shows an equivalent plot for the source 1/detector 1 pair (Fig. 1, dashed circle), which has no nearby region of MR activation. Instead, the MR region of interest was chosen to be homologous to the one for Fig. 2 (i.e., four voxels at an equivalent depth and distance from source 1/detector 1).

Next, we averaged over the eight blocks of motor activity evident in Fig. 2, converted the averages to oxy- and deoxyhemoglobin concentrations using the MBLL (Eq. (2), $B = 6$ for both 786 and 830 nm). In Fig. 4A we plot the results of this process for the 3-Hz data seen in Fig. 2, as well as the data from the 2-Hz motor rate from the same subject (Fig. 2). Heart-rate modu-

lation is still visible, in part because quasiperiodic signals are difficult to suppress using simple averaging (cf. Gratton and Corballis, 1995). In this case, the averaged BOLD signal (black) was amplitude-scaled and plotted twice for comparison purposes: once to match the HbO₂ trace and once to match the HbR trace.

In order to quantify the correspondence between BOLD and optical signals, 1-s portions of the optical time series surrounding each BOLD time point were collapsed, to reduce the HbR and HbO₂ signals to the BOLD time base. These data were collected for all three subjects at all three motor rates and the reciprocal of the BOLD signal (1/BOLD, in percentage change units) was then correlated with the computed changes in [HbR] and [HbO₂] and with the sum of these, [HbT]. The reciprocal measure was used to allow partial comparison with previous work showing that [HbR] correlates well with R_2^* (=$1/T_2^*$, which in our case is approximately 1/BOLD because gradient-echo BOLD is a T_2^*-weighted measurement).

Scatterplots of the resulting Δ(1/BOLD) vs Δ[HbR] and vs Δ[HbO₂], and the corresponding Pearson correlation coefficients (*r*), appear in Fig. 5. Again, a DPF of 6 was used in the MBLL concentration calculations for both 786 and 830 nm. The correlation with [HbO₂] is clearly stronger than with [HbR]. Three regression lines are plotted on each plot, one per subject, from which one sees that the correlation with Δ[HbR] differs dramatically across the three subjects and even for different trials from a single subject (compare subject 1 at 1 Hz—blue circles—with the other two rates from the same subject).

We hypothesized that these differences are related to a partial volume effect (Boas *et al.,* 2001) and therefore assumed that there was a different partial volume of activation across subjects as well as across tasks within a subject (which was visible in the fMRI maps; data not shown). To account for this difference, a normalization procedure was applied to the data. For each motor-rate time course from each subject, the MBLL-calculated concentrations were divided by a single nor-
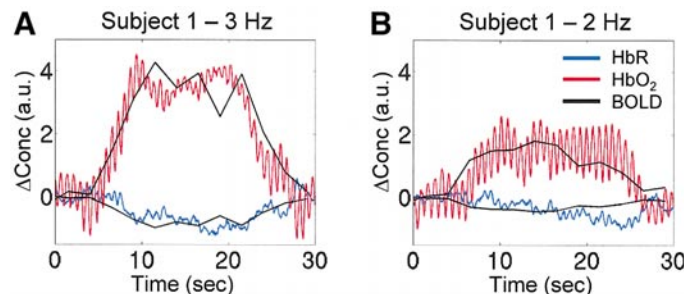

FIG. 4. Two examples of block-averaged signals (*n* = 8 blocks) during motor activation (horizontal bar). Curves are for Δ[HbO₂], Δ[HbR], and two versions of the Δ(1/BOLD) signal (amplitude-scaled to match the HbR and HbO₂ curves).

malization factor: the ratio of $\Delta[HbX]_{ON}/\Delta(1/BOLD_{ON})$, where $\Delta[HbX]_{ON}$ was an average of the last three (decimated) time points during the motor activity period for the HbX species, and $\Delta(1/BOLD_{ON})$ was an average of the corresponding BOLD time points for the associated subject at the that motor rate. This normalized each time series so that a unit percentage change in (1/BOLD) corresponded to a unit concentration change in HbX. Different normalization factors were used for each combination of subject and motor rate because we expected differences in activation volume sizes, shapes, and locations with respect to the optical probe across subjects, due to between-subject variability and also due to performance rate (Rao *et al.,* 1996).

The resulting normalized scatterplots of $\Delta[HbR]$, $\Delta[HbO_2]$, and $\Delta[HbT]$ with the $\Delta(1/BOLD)$ signals—again using DPFs of 6 and 6—appear in Fig. 6, middle row. The normalization process clearly improved the correlation with [HbR], while having substantially less impact on that with HbO_2. The plots for HbR appear twice: once with a 10-fold expanded *y* axis range showing all the data points and once on the same scale as the HbO_2 and HbT plots—which thereby excludes extreme data points. This was necessary only for HbR.

To evaluate the effect of the choice of DPF parameters on the normalized data, two additional DPF pairs were used for the calculations of $\Delta[HbR]$ and $\Delta[HbO_2]$. For convenience, the DPF for 830 nm was kept constant at a nominal value of 6 (Duncan *et al.,* 1995, 1996; Kohl *et al.,* 1998). The DPF for 786 nm was varied ±20% from this value, resulting in DPF pairs of (7.2, 6) in the top row of Fig. 6 and (4.8, 6) in the bottom row. A variation of 20% was considered a physiologically reasonable variation, as well as within the typical noise range of a direct DPF measurement.

Variations in the DPF produced little effect on the $\Delta[HbT]$ correlation with $\Delta(1/BOLD)$, an intermediate effect on the $\Delta[HbO_2]$ correlation (more movement of individual HbO_2 points relative to HbT points), and a dramatic effect on that with $\Delta[HbR]$. In the case of HbR, the best overall correlation was obtained with DPF of 4.8 and 6 (bottom row). This choice of DPF did not produce the best correlation for every combination of subject and rate, however, as seen in Table 1. For example, subject 2 had the strongest HbR correlations for 1- and 3-Hz rates (-0.81 and -0.67, respectively) using 7.2 and 6, while subject 3 had the strongest HbR correlations for 2 Hz using DPF of 6 and 6. Recalculating the overall correlation coefficients based on the best DPF pair for each subject–rate improved the correlation for HbR ($r = -0.76$, $P \ll 10^{-7}$), while those for HbO_2 and HbT remained unchanged ($r = 0.91$ and 0.82, respectively; $P \ll 10^{-7}$).

To examine the spatial sensitivity of our optical measurements, we increased the size of the MR sampling volume for each subject. Instead of selecting only statistically activated voxels, we chose a large block of voxels located below and between each source–detector pair considered. This volume reached from the surface of the head to approximately 9 mm (3 voxels) deep into cortex and spanned one voxel anterior, posterior, medial, and lateral to the source–detector pair. These regions all included the statistically activated voxels originally selected. A comparison of the two sets of correlation results appears in Table 2, illustrating that the effect of the nonactivated voxels was essentially negligible.

DISCUSSION

In this experiment, we quantified the correspondences of $\Delta(1/BOLD)$ with MBLL-derived values of $\Delta[HbR]$, $\Delta[HbO_2]$, and $\Delta[HbT]$ from noninvasive adult human NIRS recordings. Variable correlations were initially obtained, suggesting the need to account for individual differences in our calculations. After accounting for such effects, strong correlations were found between BOLD changes and all optical measures, but with systematic differences across hemoglobin species.

BOLD–HbX Correlations

We initially anticipated that changes in the BOLD signal would show the most robust correlation with changes in the concentration of deoxyhemoglobin, given that the BOLD signal arises directly from changes in the concentration of this species. While we found strong correlations for all three hemoglobin species with BOLD, the correlation with $\Delta[HbR]$ was the weakest of the three, perhaps due to its poorer contrast-to-noise ratio (CNR). To further explore our findings, we turn to the hemodynamic response to neuronal activation.

The prototypical hemodynamic response exhibits an increase in blood flow to an active region beginning within 1–3 s of the onset of activation, and a concomitant focal increase in blood volume. One consequence of this response is a focal decrease in HbR concentration, which is detected as a spatially localized increase in BOLD signal. The increase in blood volume itself, therefore, is closely associated with the BOLD signal, as observed in contrast-mediated MRI studies of cerebral blood volume (Mandeville *et al.,* 1998) and exposed cortex optical studies of functional brain activation (Malonek *et al.,* 1997; Jones *et al.,* 2001) in rats. One should therefore anticipate a correlation between HbT concentration changes and BOLD signal changes inasmuch as HbT follows blood volume. In the present study, $\Delta(1/BOLD)$ correlated strongly with $\Delta[HbT]$, with a correlation ($r \approx -0.8$) that was robust to DPF variation. The relative independence of HbT from DPF changes agrees with recent work in diffuse optics suggesting that pairing 830 nm with a second wavelength

in the range of 770–790 nm will be good for total hemoglobin measurement, when considering both random errors (Yamashita *et al.,* 2001) and systematic errors (Strangman *et al.,* 2002).

The same hemodynamic model would also predict a substantial correlation between BOLD and HbO_2 measures because the increase in volume (and HbT) is achieved entirely by a corresponding increase in HbO_2. A strong correlation of $\Delta(1/BOLD)$ with $\Delta[HbO_2]$ was indeed found, and this correlation ($r \approx -0.9$) was in fact consistently the strongest and also robust to variations in DPF.

Finally, compared to the other two hemoglobin species, an unexpectedly lower correlation of $\Delta(1/BOLD)$ to $\Delta[HbR]$ was in evidence. Previous animal work, for example, found a tight correlation ($r = 0.95$) between quantitative R_2^* ($=1/T_2^*$) and NIRS-based [HbR] changes (Punwani *et al.,* 1997, 1998), which is in agreement with existing models of the BOLD signal (Ogawa *et al.,* 1993; Buxton *et al.,* 1998; Zhong *et al.,* 1998; Hoge *et al.,* 1999) that imply that the BOLD contrast arises from magnetic disturbances caused by deoxyhemoglobin.

However, it has been argued that changes in HbO_2 are substantially larger in amplitude than HbR changes and perhaps spatially as well (e.g., Franceschini *et al.,* 2000; Shtoyerman *et al.,* 2000; Hirth *et al.,* 1996). As a result, any random errors in the optical measurements will disproportionately affect HbR. Furthermore, any cross-talk-related errors in oxygenation calculations (Boas *et al.,* 2001) will be larger from the species exhibiting a larger change into the species exhibiting a smaller change—HbO_2 into HbR, in this case—making HbR the most sensitive component to all wavelength-related errors. In fact, it has recently been found experimentally that pairing 830 nm with a second wavelength in the range of 770–800 nm would be singularly poor for oxygenation measurement—both for random errors (Yamashita *et al.,* 2001) and for systematic errors (Strangman *et al.,* 2002). This is consistent with our finding of a strong $\Delta[HbR]$ dependence on DPF. We also note that the correlations in Table 1 changed systematically as a function of the chosen DPFs, being affected primarily by one subject–rate at one DPF and by another subject–rate at another DPF (see also Fig. 6, first column). Such systematicity is also consistent with wavelength-related errors; a DPF pair that is more appropriate for one subject–rate may not be appropriate for another subject–rate even when using the same recording wavelengths. The sensitivity of calculated hemoglobin species concentrations at these wavelengths is an important experimental observation for future NIRS-based recordings, given the low cost and common use (including in commercial instruments) of lasers at 770–800 and 830 nm.

The nature of the hemodynamic changes and the wavelengths employed would therefore suggest that HbO_2, at least in this case, is a more robust hemodynamic signal—and hence more reliably correlated with BOLD-related changes—than HbR. That is, the nature of the optical measurement tends to produce a HbR signal with a low CNR, an effect that outweighs the expected closer correspondence between HbR and BOLD. Since HbT is equal to the sum of HbO_2 and HbR, one would expect HbT to have an intermediate correlation with BOLD changes, as was also found. All correlations were substantially lower than found invasively by Punwani, but there are two important methodological differences to consider. First, the animal work employed graded hypoxia instead of functional brain activation as the stimulus, and therefore the changes in HbR concentration achieved in the present paper span a much smaller range than those induced by hypoxia. Second, the previous work compared quantitative R_2^* to invasively measured [HbR], and the invasive optical measurement may provide better quantitative [HbR] values due to smaller partial volume effects.

Finally, one must consider the issues of background physiological variation as a contributor to the recorded signals and correlations. Background physiological variations (e.g., those one would observe under extended periods of passive resting conditions) are often evident in optical signals during functional tasks (e.g., Fig. 2). Several types of such signals have been characterized, including heart rate (Gratton and Corballis, 1995), Mayer waves, and "very low frequency oscillations" (Obrig *et al.,* 2000). These signals are typically stronger in the HbO_2 signal than in the HbR signal (e.g., Fig. 4). Given the known dependence of the BOLD signal on HbR, one would therefore expect non-task-related variation to enhance the correlation between BOLD and HbR relative to that between BOLD and HbO_2. Nevertheless, the BOLD–HbO_2 correlation was consistently the strongest.

While we believe the CNR for HbR to be a major contributor to the MR–optical correspondences we found, there are nevertheless systematic differences between the optical and the MR measures that should be considered, as they would remain important even given identical CNRs for HbO_2 and HbR. Systematic differences could arise from several factors, including the nature of the MR signal as well as issues associated with optical data analysis. We will consider these in turn.
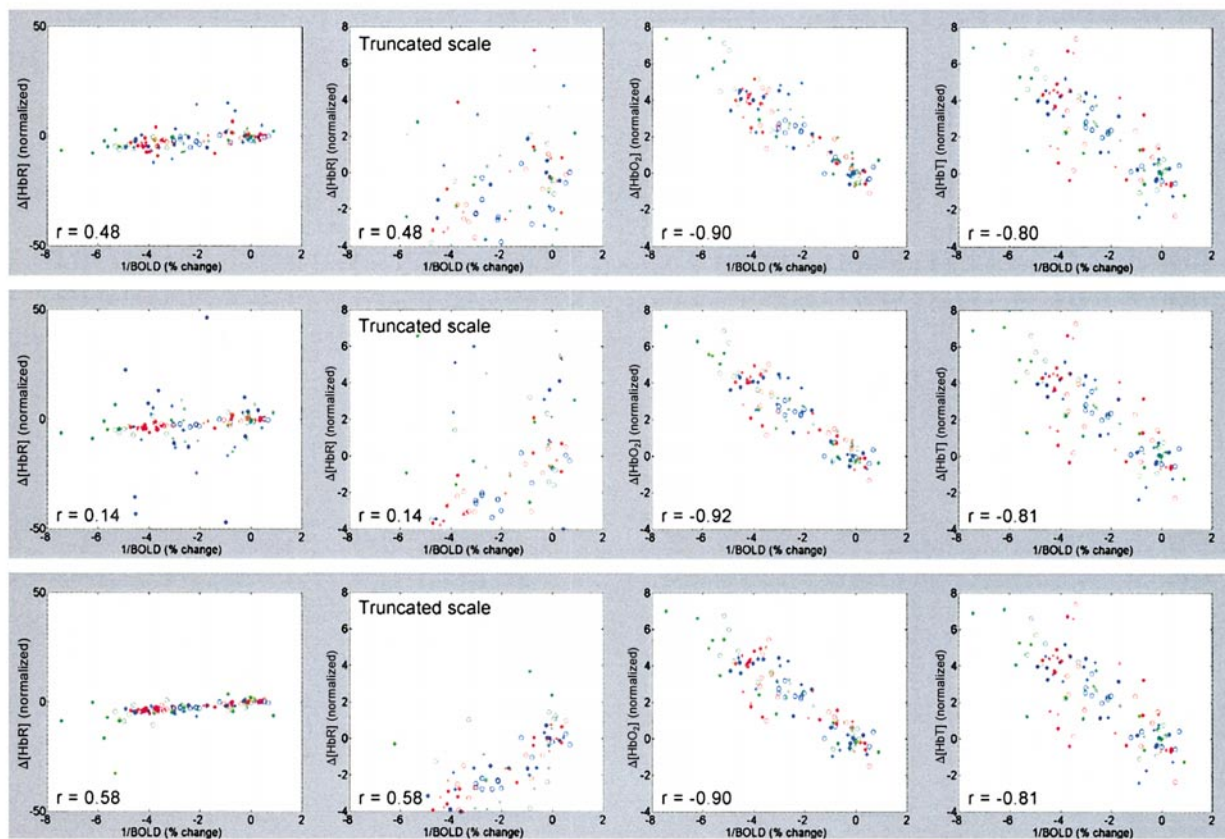
Signal Comparison Issues

MRI

First we consider the vessel sensitivity of our gradient echo BOLD sequence as a factor when comparing $\Delta[HbX]$ and $\Delta(1/BOLD)$. The type of fMR pulse sequence employed here is commonly used in functional activation experiments and produces T_2^*-weighted im-
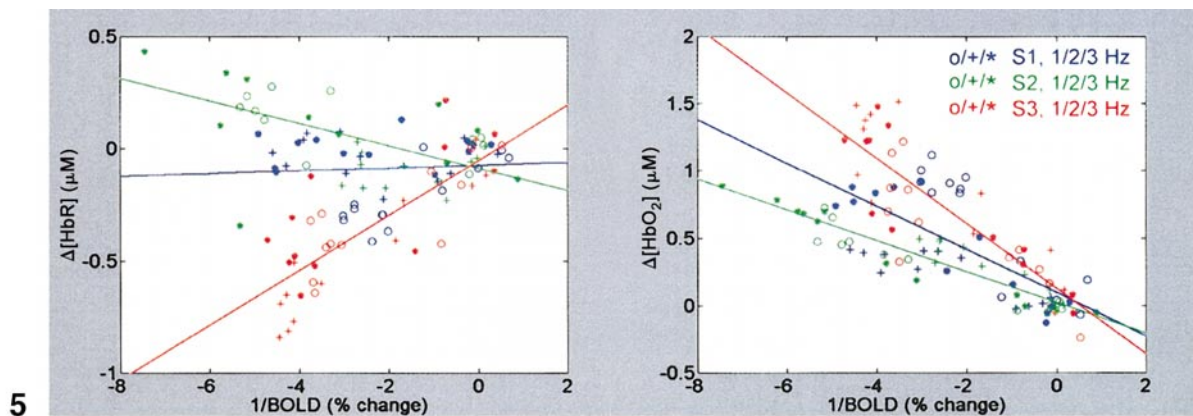
FIG. 5. Scatterplots of Δ[HbR] vs Δ(1/BOLD) and Δ[HbO₂] vs Δ(1/BOLD) prior to normalization, using DPFs of 6 and 6.

FIG. 6. Normalized scatterplots of Δ[HbR], Δ[HbO₂], and Δ[HbT] vs Δ(1/BOLD) at three DPF pairs. Top: DPF = 6 and 7.2 for 785 and 830 nm, respectively. Middle: DPF = 6 and 6. Bottom: DPF = 6 and 4.8. All correlations are significant ($P < 10^{-7}$) except HbR for DPF of 6 and 6 ($r = 0.14$, $P > 0.05$).

ages. Given our TR of 2.5 s, these images should be relatively free of T_1 "inflow" effects, since this TR is approximately five times the average T_1 of brain tissue. Neglecting nuisance effects such as shim errors and motion, the obtained images should therefore reflect predominantly T_2^* changes. These changes result from both small magnetic inhomogeneities (i.e., capillaries, at and below the 10 μm scale; T_2 effects) and inhomogeneities that are predominantly 10 μm and larger

(i.e., T_2' effects; with $1/T_2^* = 1/T_2 + 1/T_2'$). Thus, our T_2^*-weighted fMR images are sensitive, to varying degrees, to essentially all spatial scales of the vasculature. It is also the case that optical methods will be sensitive to all spatial scales (with lower sensitivity to arteries and veins larger than ~1 mm diameter, for which entering light cannot escape; Liu *et al.,* 1995). Thus, the gross spatial sensitivity of the two techniques would seem to be reasonably matched and

TABLE 1

Correlation of Δ[HbR] vs Δ(1/BOLD) for Individual Subject–Rate Combinations

Subject–rate	7.2 and 6	6 and 6	4.8 and 6
S1–R1	0.39	0.81*	**0.89***
S1–R2	0.51	−0.13	**0.63***
S1–R3	0.67*	0.13	**0.91***
S2–R1	**0.81***	0.67*	0.66*
S2–R2	0.42	0.06	**0.71***
S2–R3	**0.69***	0.51	0.45
S3–R1	0.66*	0.80*	**0.85***
S3–R2	0.90*	**0.95***	0.93*
S3–R3	0.42	0.74*	**0.92***

Note. Boldface indicates the maximum for each row; * indicates $P < 0.05$.

hence an unlikely source of signal discrepancies. In terms of compartments, BOLD is almost exclusively sensitive to the venous compartments (Lee *et al.,* 2001). While optical recordings will always be sensitive to arterial, capillary, and venous compartments, for HbR changes, optical recordings will be sensitive to the venous and capillary compartments, because that is where HbR concentration changes occur. Thus, a mismatch in spatial sensitivities of the two techniques may exist—depending on the contribution of the capillary compartment to optical changes—which could in turn affect the magnitude and robustness of HbR correlations.

It is also possible that there is a difference between our gradient-echo fMR sequences (which produce T_2^*-*weighted* images) and those sequences producing quantitative T_2^* images. The difference, however, is essentially an unknown scaling factor on the signal data for each subject. For this reason, we plotted [HbR] against the percentage change in 1/BOLD, our Δ(1/BOLD), in an attempt to compensate for these unknown scaling factors. This compensation for the T_2^*-weighting helped the correlation with all species, but the correlation between Δ[HbR] and Δ(1/BOLD) was still found to be lower than previously reported.

A third MR-related issue essentially involves the spatial extent of activation as measured by the two technologies. Standard fMRI activation maps were used to select voxels for averaging and comparison to the hemoglobin species changes. Restricting the MR analysis to voxels exhibiting changes in activity is appropriate in that the NIRS analysis is best at investigating changes in (rather than absolute) concentrations. However, identifying the proper manner by which "active" vs "inactive" regions are distinguished is not trivial (cf. Bandettini *et al.,* 1993; Friston *et al.,* 1996; Poline *et al.,* 1997). Moreover, subthreshold "activation" occurs regardless of the statistical analysis and threshold choice. For this reason, we performed an

additional comparison of each optical measure with the average MR response calculated over a much larger volume than originally considered. This larger volume included scalp, skull, and inactive brain voxels below and between the relevant source–detector pair, along with the original, statistically identified, activated voxels. The resulting correlations were virtually identical with those from the original analysis (Table 2). We therefore conclude that (i) the optical signals we recorded were predominantly or entirely brain derived as opposed to having a scalp and/or skull component and (ii) a gross spatial sensitivity mismatch is an unlikely contributor to the correlations found in our data.

NIRS

The Δ[HbX]:Δ(1/BOLD) correlations are also affected by issues related to optical data analysis. Here, the most likely contributors are the key parameters used to compute the hemoglobin species' concentrations. Given the known shortcomings in models of tissue scattering, we examined the BOLD–HbX correlations as a function of the relative DPF values. While we found a minimal dependence of Δ[HbT] and Δ[HbO₂] on the choice of DPF, we found a strong dependence of Δ[HbR] on that choice.

Overall, there are at least three potential sources of systematic error in calculated hemoglobin species concentrations. (1) For brain activation, one should expect an activation-related change to be focal and not global. The effect of this type of error is simply an unknown partial volume effect that can theoretically be corrected by multiplying a scaling factor (>1) times the calculated concentration values. (2) Light absorption and diffusion (and hence spatial sensitivity) in tissue are a function of wavelength, and as a result the different colors of light will overlap with the activated volume to different degrees. The location and spatial extent of the absorption change (e.g., due to functional activation) will change the pathlength factor depending on how the focal change intersects with a given source-detector sampling region (Boas *et al.,* 2001). (3) Some data suggest potential differences in species distribution during activation—namely, that the HbO₂ change is spatially larger than the HbR change (Hirth *et al.,* 1996; France-

TABLE 2

Correlation Coefficients of Δ[HbR], Δ[HbO₂], and Δ[HbT] vs Δ(1/BOLD) for Two Different Spatial Volumes of MR Data, Averaging across All Subjects and Rates

	Small MR volume			Large MR volume		
Species/DPF	7.2	6	4.8	7.2	6	4.8
HbR vs 1/BOLD	0.48	−0.14	0.58	0.46	−0.11	0.59
HbO₂ vs 1/BOLD	−0.90	−0.92	−0.90	−0.88	−0.90	−0.89
HbT vs 1/BOLD	−0.80	−0.81	−0.81	−0.84	−0.84	−0.85

schini *et al.,* 2000; Shtoyerman *et al.,* 2000). Properly accounting for such effects in the MBLL model would require two pathlength factors *per wavelength*—one each for HbR and HbO_2.

The first two hypothesized effects provide the justification for the applied normalization procedure, which was designed to account for differences in partial volume effects across subjects and tasks. This normalization, while partially compensating, still did not produce a correlation between HbR and 1/BOLD that matched the invasive work. To determine exactly why this might be the case will require fully merging the optical and MR modalities.

Spatial Correspondences and MR–Optical Synergy

Together, Figs. 2 and 3 demonstrate a rough spatial correspondence between MR and optical signals, as has been found previously (Kleinschmidt *et al.,* 1996; Benaron *et al.,* 2000; Toronov *et al.,* 2001a,b). While our optical equipment was sufficient to allow imaging, challenges remain for comparison of optical and MR images. In the case of brain imaging, not only are the activation regions distributed in three dimensions, but so are the optical probes and with nonuniformly varying incidence orientations. Furthermore, the tissue through which we record is not uniform but instead consists of highly nonuniform, undulating layers of optically distinct tissue types. Image reconstruction investigations, in contrast, have concentrated on reconstructions from either flat or circular, semi-infinite, uniform media (Paulsen and Jiang, 1995; Arridge and Schweiger, 1993; Pogue *et al.,* 1999), although a few more complicated geometries have been considered (e.g., Schweiger and Arridge, 1999). One consequence is relatively poor (and poorly understood) spatial resolution, particularly in depth, as found with simple NIRS measurements. The resolution issue is related to the underlying reason for our examination of multiple brain areas; no two subjects exhibited the strongest, superficial cortical activation (as determined by fMRI) in the same cortical region, and neither NIRS nor imaging methods could be used to cleanly isolate signals from the same brain region across subjects. Although the three superficial, strongly activated regions included in this study clearly respond to different aspects of the task, we assumed the correspondence between BOLD and optical signals would remain essentially invariant across cortical region, an assumption that could and should be tested in future work.

To rigorously deal with these various issues requires fully merging the optical and MR data, a process requiring three steps and for which techniques are currently being developed. First, one would segment the anatomical MR data into tissue types (e.g., air, scalp, skull, CSF, gray matter, white matter, and activated brain regions; cf. Dale *et al.,* 1999; Fischl and Dale,

2000). Given such segmentations, Monte Carlo simulations could be run to produce highly detailed sensitivity maps of photons traveling through each subject's head (e.g., Barbour *et al.,* 1995; Boas *et al.,* 2002; Pogue and Paulsen, 1998). Finally, the resulting solution to the optical forward problem can then be used to solve the full, 3D inverse optical imaging problem on complex, layered systems such as the head.

Optically, an improved scattering model arising from segmented MR data would provide a much-improved understanding of the spatial resolution of diffuse optical techniques in complex media and would also allow calculated hemoglobin concentrations to more closely represent the absolute, quantitative HbO_2, HbR, and HbT concentrations in tissue. This in turn could provide additional information on the nature of the BOLD signal and also would allow more reliable comparison of brain states over days, weeks, and months—a task that remains a formidable challenge to any existing noninvasive brain imaging method. For MR, the optical data would provide (i) a quantitative HbR benchmark for the BOLD signal; (ii) simultaneous information about HbO_2, HbR, and HbT; and (iii) improved temporal information for each of these species. When fully assembled, such information can help better illuminate the exact nature of the hemodynamic response, in general, and the BOLD signal in particular.

Implications for Interpreting BOLD and Optical Signals

In general, we were surprised to find that the best correlations were between HbO_2 and BOLD signals. We expected instead HbR and BOLD to be most strongly correlated, due to the causal relation between the presence of paramagnetic HbR and changes in the BOLD signal. We argued, however, that our findings likely resulted from the weaker CNR for HbR relative to HbO_2 in diffuse optical measures. As discussed earlier, this CNR difference arises from the smaller magnitude of the HbR response, the effect of wavelength selection (Boas *et al.,* 2001; Yamashita *et al.,* 2001), and pathlength-related cross-talk issues (Mayhew *et al.,* 1999; Kohl *et al.,* 2000; Boas *et al.,* 2001).

One important aspect of the MR–optical correlation that was not explored here is the notion of an "early response" or early, localized deoxygenation of tissue in response to functional challenge (e.g., Duong *et al.,* 2000). While this response remains controversial, a number of important papers have shown that multiple optical techniques correlate both spatially and temporally with fMRI (Menon *et al.,* 1995; Malonek and Grinvald, 1996, 1997; Vanzetta and Grinvald, 1999; Cannestra *et al.,* 2001) and that they are sensitive to this early response. Given our experimental design—a blocked paradigm and a TR of 2.5 s—our BOLD signal did not have the temporal resolution to investigate the early response and hence were almost exclusively sen-

sitive to the later response (i.e., post-flow increase and hence largely HbO_2-driven response). Interestingly, previous work has shown that (i) the spatial extent of the early response is smaller than that of the later response and (ii) HbO_2 exhibits less spatial specificity for functional activation than HbR (e.g., Hirth *et al.,* 1996). One might expect the early BOLD response and optically derived HbR signal to coincide in spatial extent, and similarly one might hypothesize that the extent of optically derived HbO_2 change and the positive BOLD response are spatially coincident. Whether this is actually the case remains to be determined (e.g., by using a many-channel, high-resolution diffuse optical probe, or using simultaneous fMRI and invasive optical imaging techniques). Finally, it is conceivable that noninvasive diffuse optical measurements will always have better CNR for HbO_2 than for HbR if, for example, it is infeasible to change or compensate for the CNR difference between the two species. The precise implications depend on whether the HbR and HbO_2 responses are spatially coincident with the early and late BOLD responses, respectively (per discussion above). It would seem, however, that the most reliable diffuse optical measures (i.e., those for HbO_2) may measure an inherently less spatially localized parameter of brain activation than BOLD. To investigate this further will first require event-related paradigms (e.g., Rosen *et al.,* 1998), which can improve both CNR and temporal resolution (particularly important for fMRI), coupled to wavelength-optimized optical measurements in a simultaneous recording paradigm. This would improve both CNR and temporal resolution for all measurements and could enable separate comparison of optical and fMRI measures for early, late, and recovery-related hemodynamic responses.

Summary

We have found strong correlations between the BOLD signal and three optically derived hemoglobin signals. After adjusting for individual differences, we found the correlation of $\Delta(1/BOLD)$ with MBLL-derived values of $\Delta[HbO_2]$ to be strongest and most robust to DPF variation, that with $\Delta[HbR]$ to be weakest and least robust, and that with $\Delta[HbT]$ to be intermediate in correlation strength but quite robust to DPF changes. Importantly, these findings remained unchanged when we included scalp, skull, and inactive brain tissue in the calculation of the average BOLD response. While these correlations may just reflect the contrast-to-noise ratios for the different hemoglobin parameters using diffuse optical methods, we discussed these findings in terms of the systematic analysis errors in the optical signal resulting from the focal nature of changes during brain activation, as well as the comparison method for MR vs optical signals. We argue that these types of errors will affect the exam-ined correlations no matter how carefully the optical measurement is made.

To study the interrelationships between these signals—particularly between the various optical signals, both spatially and temporally—our data emphasize the fact that we must better understand and deal with the systematic partial volume effects in NIRS measurements. To do so requires further investigation of (1) photon migration in complex media such as the layered, undulating, optically heterogeneous tissue layers in the head; (2) issues related to cross talk between hemoglobin species in optical data analysis; and (3) issues of spatial sensitivity including fMRI voxel selection, weighting fMRI voxels by optical sensitivities, and differing sensitivities between the two modalities due to vessel size. It is our expectation that a better understanding of these issues will eventually afford better understanding of the nature of both optical and MRI signals.

ACKNOWLEDGMENTS

REFERENCES

Adelson, P. D., Nemoto, E., Colak, A., and Painter, M. 1998. The use of near infrared spectroscopy (NIRS) in children after traumatic brain injury: A preliminary report. *Acta Neurochir. Suppl. (Wien)* **71:** 250–254.

Arridge, S. R., and Schweiger, M. 1993. Inverse methods for optical tomography. In *Information Processing in Medical Imaging* '93 (H. H. Barrett and A. F. Gmitro, Eds.), pp. 259–277. Springer–Verlag, Berlin.

Bandettini, P. A., Jesmanowicz, A., Wong, E. C., and Hyde, J. S. 1993. Processing strategies for time-course data sets in functional MRI of the human brain. *Magn. Reson. Med.* **30:** 161–173.

Barbour, R. L., Graber, H. L., Chang, J., Barbour, S. S., Koo, P. C., and Aronson R. 1995. MRI-guided optical tomography: Prospects and computation for a new imaging method. *IEEE Comput. Sci. Eng.* **2:** 63–77.

Benaron, D. A., Hintz, S. R., Villringer, A., Boas, D., Kleinschmidt, A., Frahm, J., Hirth, C., Obrig, H., van Houten, J. C., Kermit, E. L., Cheong, W. F., and Stevenson, D. K. 2000. Noninvasive functional imaging of human brain using light. *J. Cereb. Blood Flow Metab.* **20:** 469–477.

Boas, D. A., Franceschini, M. A., Dunn, A. K., and Strangman, G. 2002. Non-invasive imaging of cerebral activation with diffuse optical tomography. In *Optical Imaging of Brain Function* (R. Frostig, Ed.). CRC Press, Boca Raton, FL.

Boas, D. A., Gaudette, T., Strangman, G., Cheng, X., Marota, J. J. A., and Mandeville, J. B. 2001. The accuracy of near infrared spec-

troscopy and imaging during focal changes in cerebral hemodynamics. *NeuroImage* **13:** 76–90.

Buxton, R. B., Wong, E. C., and Frank, L. R. 1998. Dynamics of blood flow and oxygenation changes during brain activation: The balloon model. *Magn. Reson. Med.* **39:** 855–864.

Cannestra, A. F., Pouratian, N., Bookheimer, S. Y., Martin, N. A., Beckerand, D. P., and Toga, A. W. 2001. Temporal spatial differences observed by functional MRI and human intraoperative optical imaging. *Cereb. Cortex* **11:** 773–782.

Cope, M., and Delpy, D. T. 1988. System for long-term measurement of cerebral blood flow and tissue oxygenation on newborn infants by infra-red transillumination. *Med. Biol. Eng. Comput.* **26:** 289–294.

Cope, M., Delpy, D. T., Reynolds, E. O. R., Wray, S., Wyatt, J., and van der Zee, P. 1987. Methods of quantitating cerebral near infrared spectroscopy data. *Adv. Exp. Med. Biol.* **222:** 183–189.

Cope, M., van der Zee, P., Essenpreis, M., Arridge, S. R., and Delpy, D. T. 1991. Data analysis methods for near infrared spectroscopy of tissue: Problems in determining the relative cytochrome aa3 concentration. *SPIE* **1431:** 251–262.

Dale, A. M., Fischl, B., and Sereno, M. I. 1999. Cortical surface-based analysis. I. Segmentation and surface reconstruction. *NeuroImage* **9:** 179–194.

Delpy, D. T., C. M., van der Zee, P, *et al.* 1988. Estimation of optical pathlength through tissue from direct time of flight measurement. *Phys. Med. Biol.* **33:** 1433–1442.

Duncan, A., Meek, J. H., Clemence, M., Elwell, C. E., Fallon, P., Tyszezuk, L., Cope, M., and Delpy, D. T. 1996. Measurement of cranial optical path length as a function of age using phase resolved near infrared spectroscopy. *Pediatr. Res.* **39:** 889–894.

Duncan, A., Meek, J. H., Clemence, M., Elwell, C. E., Tyszezuk, L., Cope, M., and Delpy, D. T. 1995. Optical pathlength measurements on adult head, calf and forearm and the head of the newborn infant using phase resolved optical spectroscopy. *Phys. Med. Biol.* **40:** 295–304.

Duong, T. Q., Kim, D. S., Ugurbil, K., and Kim, S. G. 2000. Spatiotemporal dynamics of the BOLD fMRI signals: Toward mapping submillimeter cortical columns using the early negative response. *Magn. Reson. Med.* **44:** 231–242.

Essenpreis, M., Cope, M., Elwell, C. E., Arridge, S. R., van der Zee, P., and Delpy, D. T. 1993. Wavelength dependence of the differential pathlength factor and the log slope in time-resolved tissue spectroscopy. *Adv. Exp. Med. Biol.* **333:** 9–20.

Fantini, S., Franceschini, M. A., Fishkin, J. B., Barbieri, B., and Gratton, E. 1994. Quantitative determination of the absorption spectra of chromophores in strongly scattering media: A novel LED based technique. *Appl. Opt.* **33.**

Firbank, M., Okada, E., and Delpy, D. T. 1998. A theoretical study of the signal contribution of regions of the adult head to near-infrared spectroscopy studies of visual evoked responses. *NeuroImage* **8:** 69–78.

Fischl, B., and Dale, A. M. 2000. Measuring the thickness of the human cerebral cortex from magnetic resonance images. *Proc. Natl. Acad. Sci. USA* **97:** 11050–11055.

Franceschini, M. A., Toronov, V., Filiaci, M. E., Gratton, E., and Fantini, S. 2000. On-line optical imaging of the human brain with 160-ms temporal resolution. *Opt. Express* **6:** 49–57.

Friston, K. J., Holmes, A., Poline, J. B., Price, C. J., and Frith, C. D. 1996. Detecting activations in PET and fMRI: Levels of inference and power. *NeuroImage* **4:** 223–235.

Gratton, G., and Corballis, P. M. 1995. Removing the heart from the brain: Compensation for the pulse artifact in the photon migration signal. *Psychophysiology* **32:** 292–299.

Gratton, G., Corballis, P. M., Cho, E., Fabiani, M., and Hood, D. C. 1995. Shades of gray matter: Noninvasive optical images of human

brain responses during visual stimulation. *Psychophysiology* **32:** 505–509.

Hirth, C., Obrig, H., Villringer, K., Thiel, A., Bernarding, J., Muhlnickel, W., Flor, H., Dirnagl, U., and Villringer, A. 1996. Non-invasive functional mapping of the human motor cortex using near-infrared spectroscopy. *NeuroReport* **7:** 1977–1981.

Hock, C., Muller-Spahn, F., Schuh-Hofer, S., Hofmann, M., Dirnagl, U., and Villringer, A. 1995. Age dependency of changes in cerebral hemoglobin oxygenation during brain activation: A near-infrared spectroscopy study. *J. Cereb. Blood Flow Metab.* **15:** 1103–1108.

Hoge, R. D., Atkinson, J., Gill, B., Crelier, G., Marrett, S., and Pike, G. B. 1999. Investigation of BOLD signal dependence on CBF and $CMRO_2$: The Deoxyhemoglobin Dilution Model. *Magn. Reson. Med.* **42:** 849–863.

Homan, R. W., Herman, J., and Purdy, P. 1987. Cerebral location of international 10–20 system electrode placement. *Electroencephalogr. Clin. Neurophysiol.* **66:** 376–382.

Jobsis, F. F. 1977. Noninvasive infrared monitoring of cerebral and myocardial sufficiency and circulatory parameters. *Science* **198:** 1264–1267.

Jones, M., Berwick, J., Johnston, D., and Mayhew, J. 2001. Concurrent optical imaging spectroscopy and laser–Doppler flowmetry: The relationship between blood flow, oxygenation, and volume in rodent barrel cortex. *NeuroImage* **13:** 1002–1015.

Kleinschmidt, A., Obrig, H., Requardt, M., Merboldt, K. D., Dirnagl, U., Villringer, A., and Frahm, J. 1996. Simultaneous recording of cerebral blood oxygenation changes during human brain activation by magnetic resonance imaging and near-infrared spectroscopy. *J. Cereb. Blood Flow Metab.* **16:** 817–826.

Kohl, M., Lindauer, U., Royl, G., Kuhl, M., Gold, L., Villringer, A., and Dirnagl, U. 2000. Physical model for the spectroscopic analysis of cortical intrinsic optical signals. *Phys. Med. Biol.* **45:** 3749–3764.

Kohl, M., Nolte, C., Heekeren, H. R., Horst, S., Scholz, U., Obrig, H., and Villringer, A. 1998. Determination of the wavelength dependence of the differential pathlength factor from near-infrared pulse signals. *Phys. Med. Biol.* **43:** 1771–1782.

Lee, S. P., Duong, T. Q., Yang, G., Iadecola, C., and Kim, S. G. 2001. Relative changes of cerebral arterial and venous blood volumes during increased cerebral blood flow: Implications for BOLD fMRI. *Magn. Reson. Med.* **45:** 791–800.

Liu, H., Boas, D. A., Zhang, Y., Yodh, A. G., and Chance, B. 1995. Determination of optical properties and blood oxygenation in tissue using continuous NIR light. *Phys. Med. Biol.* **40:** 1983–1993.

Malonek, D., Dirnagl, U., Lindauer, U., Yamada, K., Kanno, I., and Grinvald, A. 1997. Vascular imprints of neuronal activity: Relationships between the dynamics of cortical blood flow, oxygenation, and volume changes following sensory stimulation. *Proc. Natl. Acad. Sci. USA* **94:** 14826–14831.

Malonek, D., and Grinvald, A. 1996. Interactions between electrical activity and cortical microcirculation revealed by imaging spectroscopy: Implications for functional brain mapping. *Science* **272:** 551–554.

Malonek, D., and Grinvald, A. 1997. Vascular regulation at sub millimeter range. Sources of intrinsic signals for high resolution optical imaging. *Adv. Exp. Med. Biol.* **413:** 215–220.

Mandeville, J. B., Marota, J. J. A., Kosofsky, B. E., Keltner, J. R., Weissleder, R., Rosen, B. R., Weisskoff, R. M. 1998. Dynamic functional imaging of relative cerebral blood volume during rat forepaw stimulation. *Magn. Reson. Med.* **39:** 615–624.

Mayhew, J., Zheng, Y., Hou, Y., Vuksanovic B., Berwick, J., Askew, S., and Coffey, P. 1999. Spectroscopic analysis of changes in remitted illumination: The response to increased neural activity in brain. *NeuroImage* **10:** 304–326.

Mayhew, J. E., Askew, S., Zheng, Y., Porrill, J., Westby, G. W., Redgrave, P., Rector, D. M., and Harper, R. M. 1996. Cerebral vasomotion: A 0.1-Hz oscillation in reflected light imaging of neural activity. *NeuroImage* **4:** 183–193.

Menon, R. S., Ogawa, S., Hu, X., Strupp, J. S., Andersen, P., and Ugurbil, K. 1995. BOLD based functional MRI at 4 Tesla includes a capillary bed contribution: Echo-planar imaging mirrors previous optical imaging using intrinsic signals. *Magn. Reson. Med.* **33:** 453–459.

Nolte, C., Kohl, M., Scholz, U., Weih, M., and Villringer, A. 1998. Characterization of the pulse signal over the human head by near infrared spectroscopy. *Adv. Exp. Med. Biol.* **454:** 115–123.

Obrig, H., Hirth, C., Junge-Hulsing, J. G., Doge, C., Wolf, T., Dirnagl, U., and Villringer, A. 1996. Cerebral oxygenation changes in response to motor stimulation. *J. Appl. Physiol.* **81:** 1174–1183.

Obrig, H., Neufang, M., Wenzel, R., Kohl, M., Steinbrink, J., Einhaupl, K., and Villringer, A. 2000. Spontaneous low frequency oscillations of cerebral hemodynamics and metabolism in human adults. *NeuroImage* **12:** 623–639.

Ogawa, S., Menon, R. S., Tank, D. W., Kim, S. G., Merkle, H., Ellermann, J. M., and Ugurbil, K. 1993. Functional brain mapping by blood oxygenation level-dependent contrast magnetic resonance imaging. A comparison of signal characteristics with a biophysical model. *Biophys. J.* **64:** 803–812.

Oldfield, R. 1971. The assessment and analysis of handedness. The Edinburgh inventory. *Neuropsychologia* **9:** 97–113.

Paulsen, K. D., and Jiang, H. 1995. Spatially varying optical property reconstruction using a finite element diffusion equation approximation. *Med. Phys.* **22:** 691–701.

Pogue, B. W., McBride, T. O., Osterberg, U. L., and Paulsen, K. D. 1999. Comparison of imaging geometries for diffuse optical tomography of tissue. *Opt. Express* **4.**

Pogue, B. W., and Paulsen, K. D. 1998. High-resolution near-infrared tomographic imaging simulations of the rat cranium by use of a priori magnetic resonance imaging structural information. *Opt. Lett.* **23:** 1716–1718.

Poline, J. B., Worsley, K. J., Evans, A. C., and Friston, K. J. 1997. Combining spatial extent and peak intensity to test for activations in functional imaging. *NeuroImage* **5:** 83–96.

Punwani, S., Cooper, C. E., Clemence, M., Penrice, J., Amess, P., Thorton, J., and Ordidge, R. J. 1997. Correlation between absolute deoxyhaemoglobin [dHb] measured by near infrared spectroscopy (NIRS) and absolute R2′ as determined by magnetic resonance imaging (MRI). *Adv. Exp. Med. Biol.* **413:** 129–137.

Punwani, S., Ordidge, R. J., Cooper, C. E., Amess, P., and Clemence, M. 1998. MRI measurements of cerebral deoxyhaemoglobin concentration [dHb]—Correlation with near infrared spectroscopy (NIRS). *NMR Biomed.* **11:** 281–289.

Rao, S. M., Bandettini, P. A., Binder, J. R., Bobholz, J. A., Hammeke, T. A., Stein, E. A., and Hyde, J. S. 1996. Relationship between finger movement rate and functional magnetic resonance signal change in human primary motor cortex. *J. Cereb. Blood Flow Metab.* **16:** 1250–1254.

Rosen, B. R., Buckner, R. L., and Dale, A. M. 1998. Event-related functional MRI: Past, present, and future. *Proc. Natl. Acad. Sci. USA* **95:** 773–780.

Schweiger, M., and Arridge, S. R. 1999. Optical tomographic reconstruction in a complex head model using a priori region boundary information. *Phys. Med. Biol.* **44:** 2703–2721.

Sfareni, R., Boffi, A., Quaresima, V., and Ferrari, M. 1997. Near infrared absorption spectra of human deoxy- and oxyhaemoglobin in the temperature range 20–40 degrees C. *Biochim. Biophys. Acta* **1340:** 165–169.

Shtoyerman, E., Arieli, A., Slovin, H., Vanzetta, I., and Grinvald, A. 2000. Long-term optical imaging and spectroscopy reveal mechanisms underlying the intrinsic signal and stability of cortical maps in V1 of behaving monkeys. *J. Neurosci.* **20:** 8111–8121.

Simpson, C. R., Kohl, M., Essenpreis, M., and Cope, M. 1998. Near-infrared optical properties of ex vivo human skin and subcutaneous tissues measured using the Monte Carlo inversion technique. *Phys. Med. Biol.* **43:** 2465–2478.

Steinmetz, H., Furst, G., and Meyer, B. U. 1989. Craniocerebral topography within the international 10–20 system. *Electroencephalogr. Clin. Neurophysiol.* **72:** 499–506.

Strangman, G., Franceschini, M. A., and Boas, D. A. 2002. Factors affecting the accuracy of near-infrared spectroscopy (NIRS) data analysis for focal changes in hemodynamics. Submitted for publication.

Taylor, J. A., Williams, T. D., Seals, D. R., and Davy, K. P. 1998. Low-frequency arterial pressure fluctuations do not reflect sympathetic outflow: Gender and age differences. *Am. J. Physiol.* **274:** H1194–1201.

Toronov, V., Webb, A., Choi, J. H., Wolf, M., Michalos, A., Gratton, E., and Hueber, D. 2001a. Investigation of human brain hemodynamics by simultaneous near-infrared spectroscopy and functional magnetic resonance imaging. *Med. Phys.* **28:** 521–527.

Toronov, V., Webb, A., Choi, J. H., Wolf, M., Safonova, L., Wolf, U., and Gratton, E. 2001b. Study of local cerebral hemodynamics by frequency-domain near-infrared spectroscopy and correlation with simultaneously acquired functional magnetic resonance imaging. *Opt. Express* **9:** 417–427.

Vanzetta, I., and Grinvald, A. 1999. Increased cortical oxidative metabolism due to sensory stimulation: Implications for functional brain imaging. *Science* **286:** 1555–1558.

Wolf, T., Lindauer, U., Reuter, U., Back, T., Villringer, A., Einhaupl, K., and Dirnagl, U. 1997. Noninvasive near infrared spectroscopy monitoring of regional cerebral blood oxygenation changes during peri-infarct depolarizations in focal cerebral ischemia in the rat. *J. Cereb. Blood Flow Metab.* **17:** 950–954.

Wray, S., Cope, M., and Delpy, D. T. 1988. Characteristics of the near infrared absorption spectra of cytochrome aa3 and hemoglobin for the noninvasive monitoring of cerebral oxygenation. *Biochim. Biophys. Acta* **933:** 184–192.

Yamashita, Y., Maki, A., and Koizumi, H. 2001. Wavelength dependence of the precision of noninvasive optical measurement of oxy-, deoxy-, and total-hemoglobin concentration. *Med. Phys.* **28:** 1108–1114.

Zhong, J., Kennan, R. P., Fulbright, R. K., and Gore, J. C. 1998. Quantification of intravascular and extravascular contributions to BOLD effects induced by alteration in oxygenation or intravascular contrast agents. *Magn. Reson. Med.* **40:** 526–536.